To be published in the IEEE Trans. on Nuclear Science (December 1994)

Clementine RRELAX SRAM Particle Spectrometer

M. G. Buehler, G. A. Soli, B. R. Blaes, J. M. Ratliff,
and H. B. Garrett

Jet Propulsion Laboratory
California Institute of Technology
Pasadena, CA91109

ABSTRACT

The Clementine RRELAX radiation monitor chip consists of a p-FET total dose monitor and a 4-kbit SRAM particle spectrometer. Eight of these chips were included in the RRELAX and used to detect the passage of the Clementine (S/C) and the innerstage adapter (ISA) through the earth's radiation belts and the 21-Feb 1994 solar flare. This is the first space flight for this 1.2-Inn rad-soft custom CMOS radiation monitor. This paper emphasizes results from the SRAM particle detector which showed that it (a) has a detection range of five orders of magnitude relative to the 21-Feb solar flare, (b) is not affected by electrons, and (c) detected microf l ares occurring with a 26.5-day period,

1. INTRODUC ION

The Clement ne spacecraft was launched January ?5, 1994 (day 25) from Vandenberg Air Force Base on a Titan IIG booster. The spacecraft, shown in Fig. 1, contains a number of advanced light weight cameras used to photograph the moon during its 2.4-ninth lunar orbit. The S/C and ISA also contain a RRELAX (Radiation and Reliability Assurance Experiment) which was located on the S/C and ISA as seen in Fig. 1.

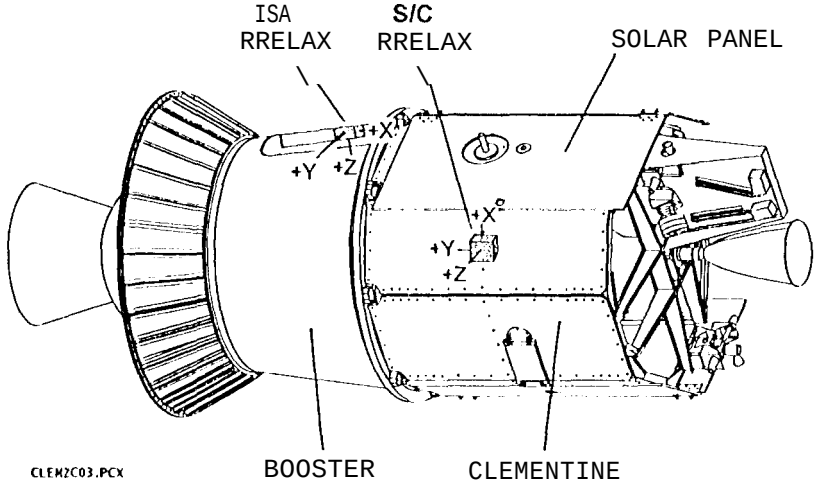

Figure 1. Launch configuration for the Clementine spacecraft (S/C) and the inner stage adapter (ISA) with a RRELAX box mounted on each. TheS/C RRELAX is actually located on the opposite panel.

The tots' dose profile for the S/C is shown in Fig. 2. These measurement were obtained from p-FETs which were measured with a constant current set to the temperature-insensitive point [1]. The figure shows the passage of the S/C through the earth's electron belt followed by moon orbit which began on day 50, Shortly after beginning moon orbit, a solar flare was encountered on day 52. After leaving the moon on day 123 the S/C again passed through the earth's radiation belt and shortly thereafter ceased operation.

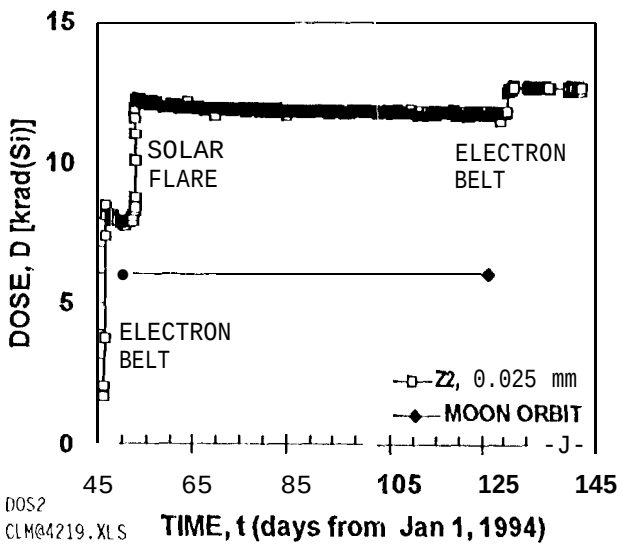

Figure 2, Overview of the S/C p-FET dose profile for lightly shielded device 22.

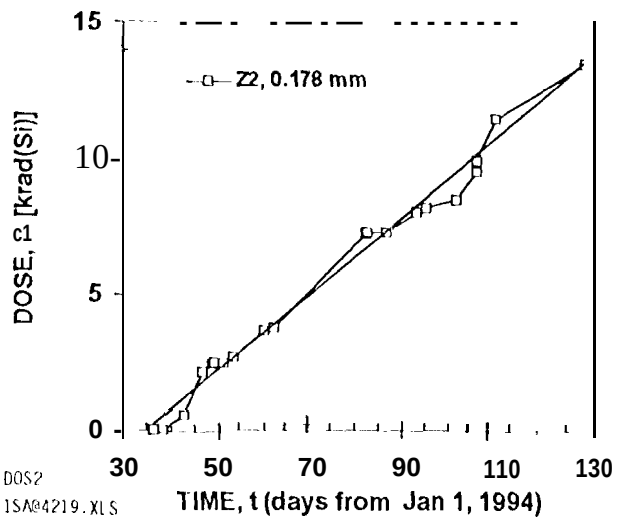

Figure 3 Overview of the ISA p-FET dose profile for lightly shielded device Z2.

The total dose profile for the ISA is shown in Fig. 3. l-he ISA was in a 2.1-day earth orbit from Feb 4 (day 35) until it recentered the atmosphere on about May 8 (day 128). During this time it experienced essentially a linear increase in total dose as shown in Fig. 3. The solar flare was not visible in the ISA p-FET data because the ISA is more heavily shielded than the S/C.

2. RRELAX

lhe RRELAX is a 624 g, 2.4 watt microprocessor controlled experiment, shown in Fig. 4, that contains 166 test devices designed to evaluate the effects of radiation and the thermal environment on the performance of these devices. This paper discusses results from six RADMONs (Radiation Monitors), 22, 23, 25, 24, Xl, and Y1 mounted on X-, Y-, and Z- faces of the RRELAX.

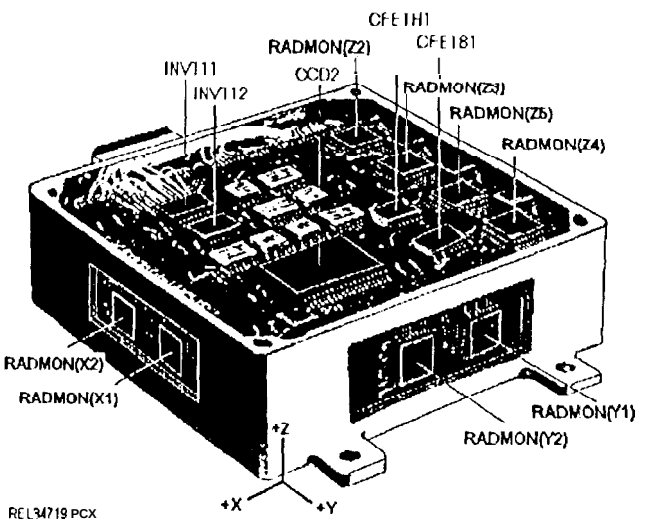

Figure 4. RRELAX components arranged in a 10.2 cm x 10.2 cm x 3.8 cmbox.

3. SRAM PARTICLE SPECTROMETER

The RADMON chip, shown in Fig. 5, was fabricated in 1.2-μm radiation-soft CMOS. The chip is a full custom designed chip that contains seven components. In this paper only the results from the p-FET and the 4-kbit SRAM are presented. The p-FET was used to determine the total radiation dose and the SRAM was used to determine the particle flux.

lhe SRAM as a particle detector enhances the single-event -upset (SEU) effect that is detrimental to SRAMs when used as memory elements [2]. The SRAM has a six-transistor cell with an offset voltage, V_o, to adjust the sensitivity of the cell to particle upsets induced by for example protons [3] or alpha particles [4]. In addition, the sensitive drain of the n-FET was bloated to A_0 = 42.1 μm^2 so the 4-kbit SRAM active area is 0.0017 cm^2.

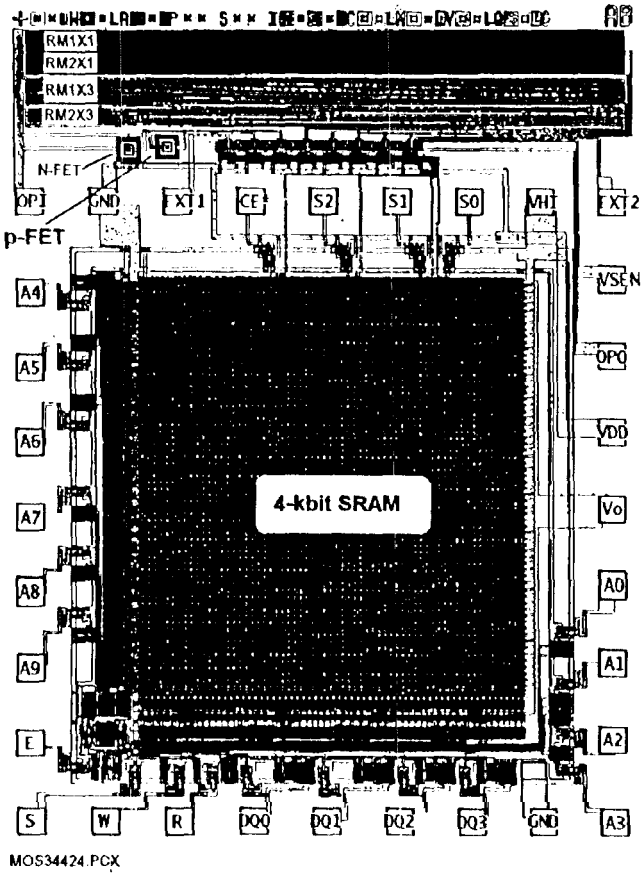

Figure 5. RADMON chip 2.6 x 3.4 mm^2 fabricated in 1.2-μm CMOS contains both a p-FET total dose monitor and an SRAM particle detector.

The calibration of the cell, shown in Fig. 6, used both protons and alpha particles, The experimental data points were obtained at various incident ion energies, E2, for an offset voltage that corresponds to a cross section of $A_0/2$. The cross section is the upset rate divided by the particle flux times the number of cells which is 4096 in this case. The solid lines were fitted to the experimental data using the deposited ion energy derived from the range-energy curves [5]. These calculations require the overlayer thickness, DX3, and the collection layer thickness DX4, Values for these thicknesses are shown in the figure. The deposited energy is expressed as the difference between the energy at the start of the collection layer, E3, and the energy at the end of the collection layer, E4. During the rising portion of the curve, the ions stop in the collection layer and so E4 = O. Finally, the offset voltages are stated relative to the spontaneous offset voltage $V_{os\mu}$ = 1.148 V.

lhe SRAM was operated with two threshold voltages which were 0.15 V and 1.0 V above the spontaneous upset point, $V_{os\mu}$. As seen in Fig. 6 for DV_o = 0.15 V, protons in the 0.55 to 0,8 MeV range can upset the SRAM and alpha particles with energies above 1.8 MeV can upset the SRAM. When operated with this threshold, the SRAM is said to be sensitive to particles with atomic numbers of Z≥1. For DV_o = 1.0 V only heavy ions such as oxygen or iron can upset the SRAM.

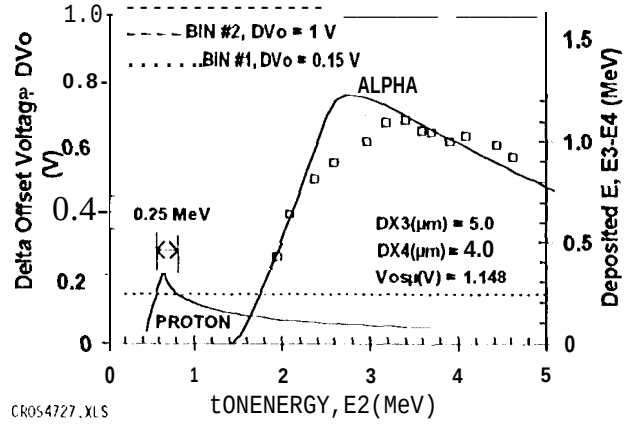

Figure 6. Calibration curves and operational thresholds for the SRAM particle detector.

In operation [6], the SRAM is written with ones with V. = VDD = 5 V. Then V. is lowered to a value DV_o above $V_{os\mu}$ for a stare period of 100 s. Then V. is returned to VDD and the number of zeros or particle flipped cells read. In addition to lowering V_o, the VDD for the chip was also lowered to 3 V to reduce the chip power consumption. During satellite operation,

each SRAM was operated for 100 s with DV_o = 0.15 V and then for 100 swith DVo= 1 V. This cycle was continued for 1 hour. The number of upsets reported is the sum of the upsets recorded during the 18 x 100 s = 30 minutes that the SRAM spent in each state,

The RADMONs were shielded by different lids as listed in Table 1, The devices were packaged

Table 1. Shields in mm and Normal Incident Proton Energy in MeV.

DEV NO.	S/C LIDS	S/C mm	S/C mil	S/C MeV	ISA mm	ISA mil	ISA Mev
2.2	0	0.025	1	1.3	0,178	7	4,6
23	1	0.787	31	11.4	0.940	37	12.7
25	2	1.549	61	16.9	1.702	67	17.8
24	3	2.311	9121.1		2.464	97	21.9
xl	1	0.787	31	11.4	0.940	37	12.7
Y1	1	0,787	31	11.4	0.940	37	12.7

with an integral number of 0.25-mm Kovar lids. A conversion factor of three was used to convert Kovar thickness to Al thickness, That is 1 mm of Kovar is equivalent to 3 mm of Al. The O-lid device was covered with 13-μm Al-coated Kapton and the RRELAX box was similarly covered with this Kapton. Thus the O-lid device is listed as having a 25-μm Al shield. The equivalent thickness of each shield in mm and roils of Al is listed in Table 1. These numbers represent the thickness of the lid, box covering, and, for the ISA RRELAX, 0.152-mm thermal blanket.

The mean proton energy needed to penetrate the shield and upset the SRAM when operated with DV_O = 0.15 V is also listed in Table 1. The values shown in the table were obtained from proton range-energy curves [5]. The shields slow the protons so their energy is reduced to between 0.55 and 0.8 MeV when they reach the collection region of the SRAN and thus can cause an upset.

4. TEST RESULTS

An overview of the S/C and ISA SRAM particle detector data is presented in **Figs. 7 to 9** for Z≥1 and heavy ion particles. Zero upsets are shown as 0.2 upsets. The 21-Feb solar flare is clearly visible at day52 in Figs. 7 to 9.

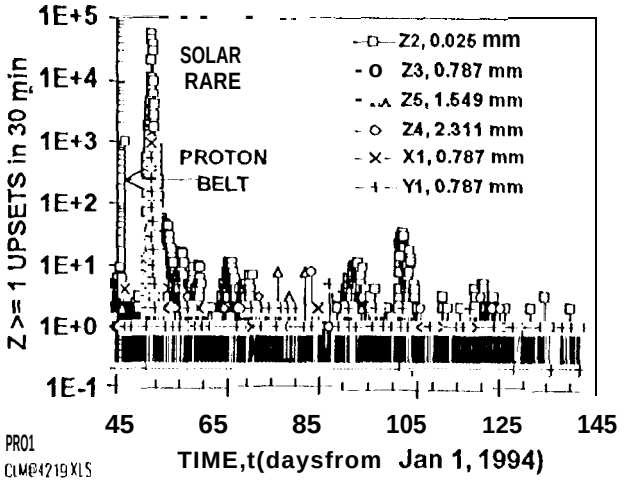

Figure 7. Overview of the Z≥1 upsets for S/C Z?, 23, 25, 24, Xl, and Y1 SRAMs.

The data shown in Fig. 8 was heavily censored for there were a great many system glitches of unknown origin on the ISA which caused massive SRAM upsets. These upsets are most likely due to noise on the power supplied to the RRELAX. Thus, a lesson learned is that the power supply must be stable especially during the 100 s stare period,

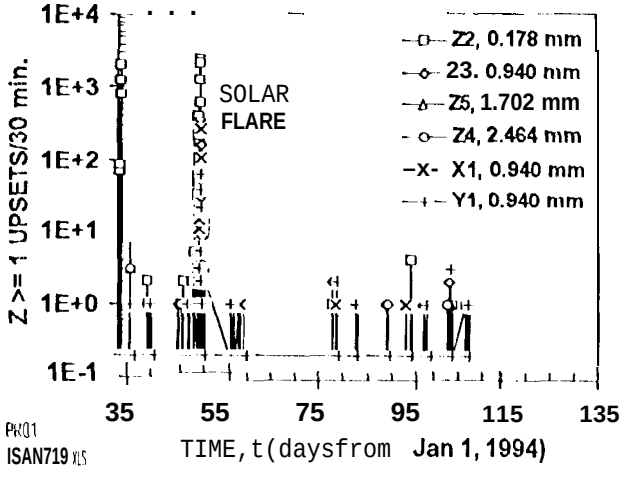

Figure 8. Overview of the Z≥1 upsets for ISA Z2, 23, 25, 24, Xl, and Y1 SRAMs.

As shown in the following figures, most upsets follow a pattern where the lightly shielded SRAMs have more upsets than the heavily shielded SRAMs. As seen in Figs. 7 to 9, this pattern is broken during quiet times when the

background radiation can upset the more heavily shielded SRAMs more often than the lightly shielded SRAMs.

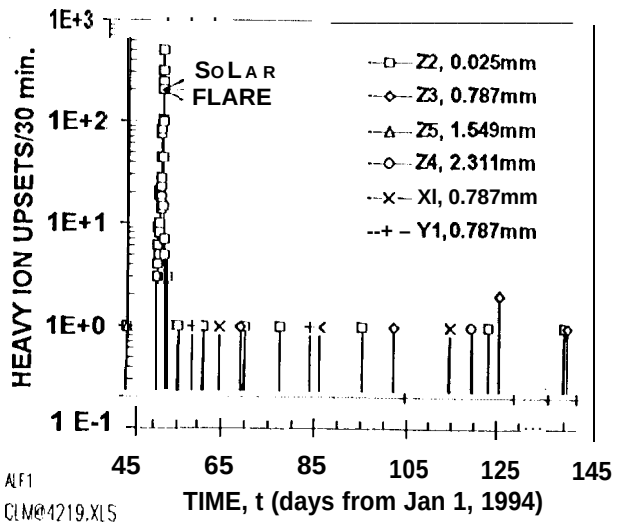

Figure 9. Overview of the heavy ion upsets for SIC 22, 23, 25, 24, Xl, and Y1 SRAMs.

The' effect of shielding on the 21-Feb solar flare is shown in Fig. 10, The shielding thickness is listed in the legend and the corresponding protons energies are listed in Table 1. The figure illustrates how the upsets decrease with shielding thickness.

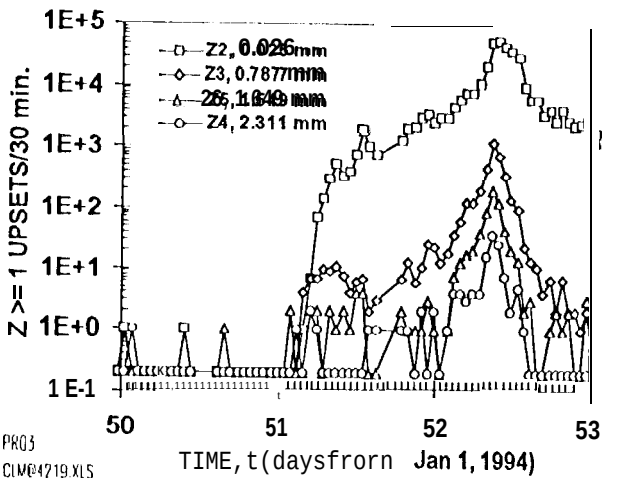

Figure 10, Effect of shielding on the upset response of the S/C 22, 23, 25, and 24 SRAMs during the 21-Feb solar flare.

The energy dependence of proton flux at the solar flare peak is shown in Fig. 11. This data was corrected for the reduction in the memory cell count during the stare cycle using $No = -N_t \cdot \ln(1 - N/N_t)$ where N_t = 18″4096 and N is the number of upsets shown in Fig. 10. The field-of-view was assumed to be π sr. As seen in Fig. 10 for 22, N = 56,503 and No = 107,202.

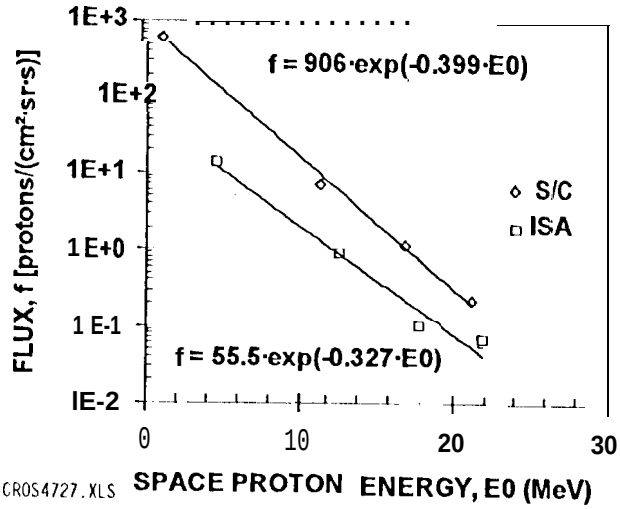

Figure 11, Peak proton flux energy dependence for the 21-Feb solar flare for S/C and ISA.

As seen in Fig. 11, the flare was more intense for the S/C than for the ISA, In comparison with other worst case flares [7], this flare was several orders of magnitude lower in its intensity.

lhe effect of orientation is shown in Figs. 12

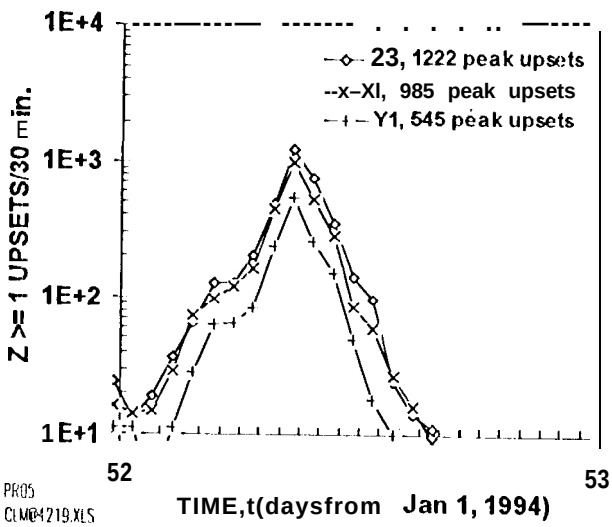

Figure 12. Effect of orientation on the upset response of the S/C 23, Xl, and Y1 SRAMs during the 21-Feb solar flare.

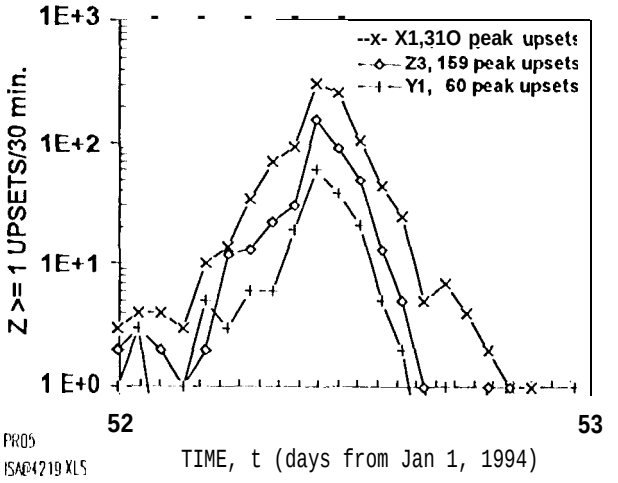

Figure 13. Effect of orientation on the upset response of the ISA 23, Xl, and Y1 SRAMs during the 21-Feb solar flare.

and 13. The ordering of the data follows approximately the field-of-view of each SRAM as seen in Fig. 1,

For the S/C, the field-of-view or solid angle for the Z-axis is approximately 2rr; whereas, for the X- and Y- axes, it is closer to *n*, Thus the Z-axis should have the most upsets but the curves for the X- and Y- axes should be closer. For the ISA, the field-of-view is largest for the X-axis and smallest for the Y-axis. The ISA contains a large spherical tank the occludes the RRELAX field-of-view. The ISA results fit intuition better than the S/C results.

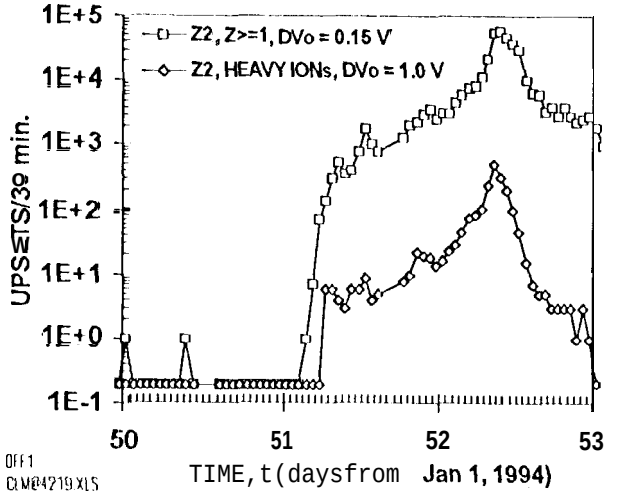

Figure 14. Effect of thresholding on the upset response of the S/C 22 SRAM during the 21-Feb solar flare.

The effect of thresholding on upsets is shown in Figs. 14 and 15. These figures indicate that the number of upsets decreases as the threshold increases. The upper curve is due to Z≥1 particles and the lower curve is due to heavy ions. This shows how the SRAM is used to electronically discriminate between light and heavy particles. In Fig 14, there is a significant shift between the light and heavy particle **responses.**

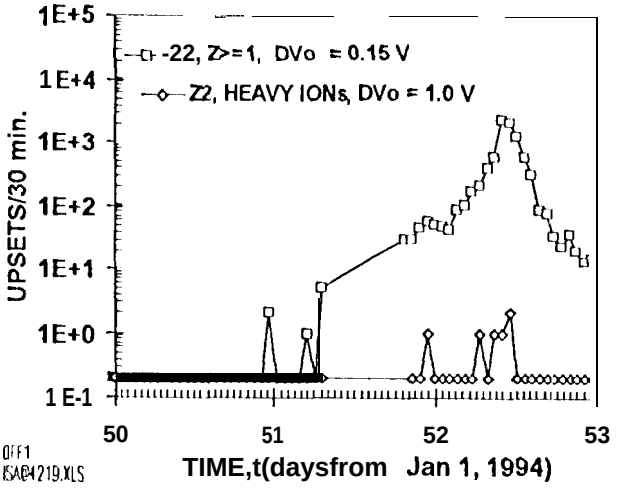

Figure 15. Effect of thresholding on the upset response of the ISA 22 SRAM during the 21-Feb solar flare.

A comparison of the p-FET and SRAM response is shown in Fig. 16 during the passage of the S/C through the earth's radiation belts. First the SRAM is upset by protons in the proton belt and then the p-FET is dosed by electrons in the electron belt. The p-FET responds to total ionizing charge; whereas, the SRAM responds only to ion strikes and not electrons.

The 21-Feb solar flare response of the S/C 23 SRAM was compared to the GOES-7 particle detector in Fig. 17. During the flare, the S/C was in moon orbit and the GOES-7 in geosynchronous orbit. This explains the one-hour shift in the responses.

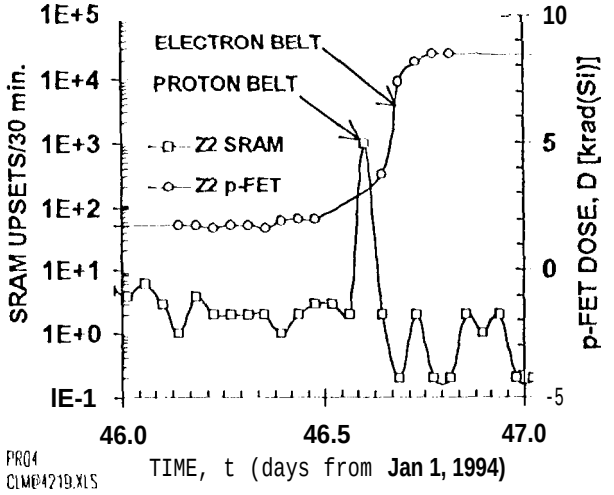

Figure 16 Response of the S/C 22 p-FET which detected the electron belt passage and the SRAM which detected the proton belt passage.

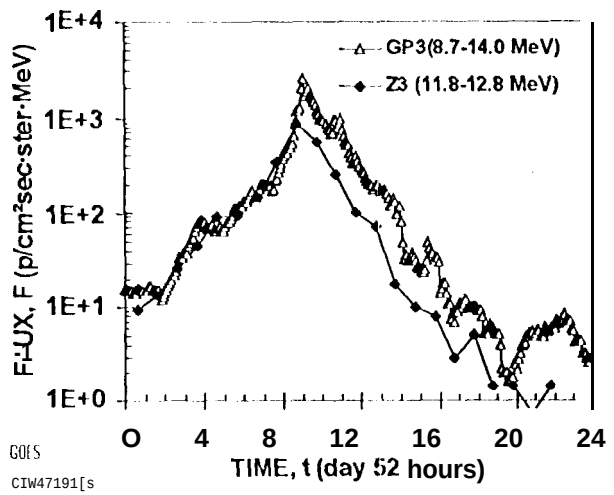

Figure 17. Comparison of the GOES-7 particle spectrometer with the S/C 23 SRAM detector.

Two microflare series are shown in Fig. 18 for the 22 SRAM. This SRAM is very lightly shielded with a 25-μm Al shield which means that it responds on the average to 1.3 MeV protons. Note the data shown in the figure was not corrected for memory cell depletion during the stare cycle.

The microflare at day 105 is apparently associated with the 21-Feb solar flare. This feature was also seen in the SAMPEX's [8] MAST [9] data as seen in Fig 19. In this figure the

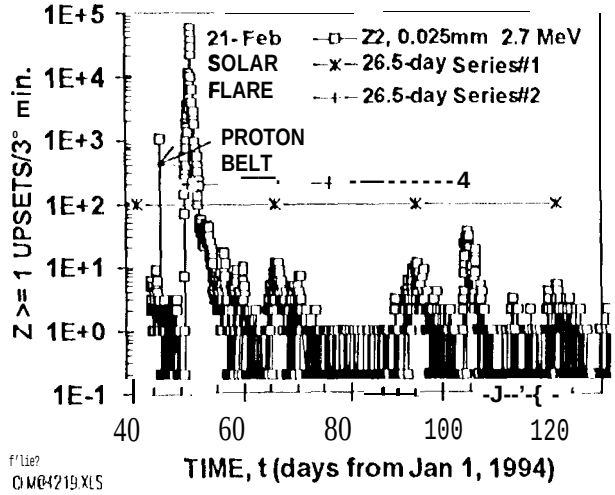

Figure 18, Microflares appear in two cycles with a 26.5-day period,

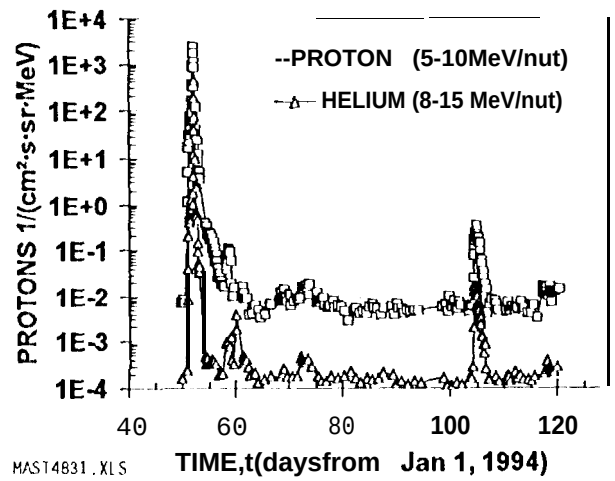

Figure 19. A microflare appears at day 1.05 in this data from the SAMPEX MAST detector. This feature is displaced by two 26.5-day periods from the 21-Feb (day 52) solar flare.

Series #2 upsets are due to both protons and helium ions. Notice that there is no microflare after the first 26.5-day period at day 78.5. The data shown in this figure was not corrected for detector dead time which will increase the flux near the solar flare peak.

The Series #1 microflares, seen in Fig. 18, were also observed by the SAMPEX'S LEICA instrument [10]. This series is composed of 0.5 - 6.6 MeV/nuc helium atoms [11].

5. DISCUSSION

The upsets, shown in Fig. 19, indicate that the SRAM has a dynamic range of five orders of magnitude relative to the 21-Feb solar flare. The response in passing through the earth's radiation belts, shown in Fig. 16, indicates that the SRAM does not respond to electrons but responds only to protons.

As seen in Fig. 7. the SRAM has most upsets when it is virtually unshielded. The active area of the SRAM is 0.00172 cm^2 which is smaller than centimeter-size pin diode and surface-barrier detectors used in particle spectrometers for measuring space background radiation particles. Because the active area of the SRAM is small, its usefulness lies in analyzing higher density particles found in solar flares and the earth's radiation belts.

The spectrometer aspects of the SRAM are determined by the shielding and V_o. Shielding filters the external particle spectrum so that only those particles that fall into the energy detection window can upset the SRAM; see Fig. 6. The offset voltage, V_o, sets the upset threshold as depicted in Fig. 6 so the SRAM can discriminate between light and heavy particles.

ACKNOWLEDGMENTS: The research described here was performed by the Center for Space Microelectronics Technology, Jet Propulsion Laboratory. California Institute of Technology, and was sponsored by the Ballistic Missile and Defense Organization, Innovative Science and Technology Office. The authors are indebted to T. Sorensen, JPL, task manager; K. Hicks, JPL, cognizant engineer; J. Pepoon, JPL parts procurement: and P. Rustan, BMDO, for his encouragement and support. Devices were fabricated through MOSIS, 1S1, USC. NSRE4721

REFERENCES:

1. M. G. Buehler, B. R. Blaes, G. A. Soli, G. R. Tardio, "On-Chip p-MOSFET Dosimetry" IEEE Trans. Nuclear Science 40, 1442-1449 (1993).

2. J. C. Pickel and T. J. Blandford, Jr. "CMOS RAM Cosmic-Ray Induced Error Rate Analysis," IEEE Trans. Nuclear Science, NS-28, 3962-3967 (1881) .

3. M. G. Buehler and B. R. Blaes, "Alpha-Particle Sensitive Test SRAMs," IEEE Trans. Nuclear Science, 37, 1849-1854 (1990).

4. G. A. Soli, B. R. Blaes, and M. G. Buehler, "Proton-Sensitive Custom SRAM Detector," IEEE Trans. Nuclear Science, 39, 1374-1378 (1992).

5. J. F. Ziegler, Handbook of Stopping Cross-Sections For Energetic Ions in All Elements (Pergamon Press, New York, 1980).

6. R, Blaes and M. G. Buehler, "SEU/SRAM as a Process Monitor" IEEE Trans. on Semiconductor Manufacturing, in press.

7. J. H, Adams and A. Gelman, "The Effects of Solar Flares on Single Event Upsets," IEEE Trans. Nuclear Science, 31, 1212-1215 (1984).

8. D. N. Baker, G. M. Masson, O. Figueroa, G. Colon, J. G. Watzin, and R. M, Aleman, "An Overview of the Solar, Anomalous, and Magnetospheric Particle Explorer (Sampex) Mission," IEEE Trans. on Geoscience and Remote Sensing, 31, 531-541 (1993).

9. W. R, Cook, A. C. Cummings, J. R. Cummings, 1. L. Garrard, B. Keeman, R. A. MeWalt, R. S. Selesnick, E. C. Stone, and T. T. von Rosenvinge, "MAST: A Mass Spectrometer Telescope for Studies of the Isotopic Composition of Solar, Anomalous, and Galactic Cosmic Ray Nuclei, "IEEE Trans. Geoscience and Remote Sensing, 31, 557-564 (1993).

10. G. M. Mason, D. C. Hamilton, P. H. Walpole, K. F. Heuerman, T. L. James, Michael H. Lennard, and J. E. Mazur, "LEICA: A Low Energy Ion Composition Analyzer for the Study of Solar and Magnetospheric Heavy Ions," IEEE Trans. Geoscience and Remote Sensing, 31, 549-556 (1993).

)1. G. M. Mason and R. S. Selesnick supplied unpublished LECIA data.